Crystallographic texture and interface structure in Co/Cu multilayer films

D. E. Joyce, C. A. Faunce, and P. J. Grundy
Department of Physics, University of Salford, Salford, M5 4WT, United Kingdom

B. D. Fulthorpe, T. P. A. Hase, I. Pape, and B. K. Tanner
Department of Physics, University of Durham, Durham, DH1 3LE, United Kingdom

(Received 15 December 1997; revised manuscript received 23 February 1998)

This paper reports on the apparent relationship between giant magnetoresistance (GMR) and crystallographic texture in sputter-deposited polycrystalline Co/Cu multilayers. In agreement with previous work, we find that GMR decreases from a typical literature value in a randomly oriented multilayer to a very low value of less than 2% in multilayers with a strongly defined ⟨111⟩ fiber texture. The change in orientation and the retained integrity of the multilayer is followed by x-ray diffraction and reflectivity, and high-resolution electron microscopy and electron diffraction. Modeling of the x-ray reflectivity data suggests that there is no significant change in the interface roughness of the multilayers with change in texture. To complement the magnetic hysteresis and GMR measurements, the transition from partially antiferromagnetic coupling to ferromagnetic coupling has been followed by polarized neutron reflectivity with *in situ* magnetization measurements.
[S0163-1829(98)05733-6]

I. INTRODUCTION

Over the last several years there has been a lively debate on the origin of the giant magnetoresistance (GMR) effect in metallic multilayers. Since its discovery in 1988 (Ref. 1) evidence has mounted that the effect arises in multilayers as a result of differences in the scattering cross sections with respect to magnetization in the two spin polarized electron populations. In antiferromagnetically coupled multilayers spin-up and spin-down electrons are s-d scattered in alternate layers into states in the split d band[2] resulting in a high resistance. In ferromagnetically coupled regions the scattering cross section for spin-up electrons is reduced causing a decrease in resistance. It has been shown[3] that the magnitude of the effect has an oscillatory dependence on the thickness of the nonmagnetic spacer layer corresponding to oscillations from ferromagnetic to antiferromagnetic coupling between the magnetic layers. Theoretical studies[4] explained this oscillatory dependence in terms of Fermi surface effects and suggested that, in the Co/Cu system, the effect should be stronger for {100} and {110} oriented films than for {111} oriented films. However, studies since then have both supported[5] and contradicted[6] this view, with particularly strong arguments coming from the disparity between some molecular-beam epitaxy (MBE) grown and sputter-deposited samples. In this difference, the second antiferromagnetic maximum has often not been observed in MBE deposited samples. It has been suggested[7] that the areal fraction coupling ferromagnetically could increase with the order of the antiferromagnetic maximum and may completely mask the higher order maxima. The relative importance of the contribution of interface scattering to GMR has also been a subject of much debate[8,9] and is thought to be very important in some cases such as Fe/Cr multilayer structures[10] in which Friedel-type scattering occurs at Cr impurity atoms in the Fe layer at the interface.

In this study, we have examined the effect of substrate etching on the magnetic, crystalline, and interfacial properties of modified polycrystalline sputter-deposited Co/Cu multilayers. In previous work[11] we have shown that substrate etching is a very effective way of controlling the crystalline orientation of sputter-deposited multilayers grown on silicon. We also showed that in those samples there was a strong apparent correlation between GMR and crystalline texture, with well developed {111} mosaic textures being associated with very low GMR. However, questions still remained as to the influence of the interfaces between the layers. In this work, with its emphasis on microstructural investigations, we show from detailed x-ray reflectivity measurements and careful modeling that, although there is a slight increase in the film roughness with etching, the change in GMR in our samples appears, again, to be largely driven by the change in preferred crystal orientation in the multilayer. In the limited range of roughness in our samples there does not appear to be an obvious correlation between interlayer roughness and GMR. These findings are corroborated by transmission electron microscopy of cross sections from the multilayers and complemented by neutron reflectivity, x-ray diffraction, and magnetization measurements.

II. EXPERIMENTAL

Films with a nominal structure of $16\times\{1\text{ nm Co}/X\text{ nm Cu}\}+1\text{ nm Pt}$, with $X=1$ nm (type A) or $X=2$ nm (type B), were grown on ion beam etched silicon (100) wafers by dc magnetron sputter deposition. In this paper we mostly concentrate on type-B multilayers which, with thicker copper spacer layers, can be prepared more reproducibly at the second maximum in the GMR vs spacer layer thickness curve.[3,11] The base pressure of the process chamber was below 10^{-5} Pa. Deposition rates at room temperature under an argon pressure of 0.4 Pa were 0.04, 0.07, and 0.08 nm per second for Co, Cu, and Pt, respectively. Before deposition the substrates were etched for 2 min using a Kaufman-type ion beam source under a 0.1 Pa pressure of argon and at

beam voltages up to 1 kV. For convenience we describe samples grown on the native SiO_2 covered Si wafers as ''unetched'' samples and those grown on substrates etched with the ion beam as ''etched.''

GMR was measured at room temperature using the standard dc four point probe method with the current and magnetic field orthogonal and in the plane of the film. The magnitude of the effect was calculated in the usual way (GMR $=100*\Delta R/R_f$, where R_f is the measured resistance in a saturation field and ΔR is the absolute difference between the zero field resistance and R_f). Magnetic hysteresis loops of the multilayers were measured on a laboratory AGFM (alternating gradient field magnetometer) at room temperature. Care was taken to minimize the effect of the alternating gradient field on the magnetic state of the sample. However, measurements near zero field remain inherently unreliable.

High angle x-ray diffraction measurements (HXRD) were carried out on a Siemens D5000 diffractometer system at copper $K\alpha$ radiation wavelengths. The system allows independent computer control of both the source and detector angles thus opening up the possibility of plotting full reciprocal space maps for each sample. High-resolution transmission electron microscope (TEM) and diffraction (TED) analyses were carried out on a JEOL 3010 microscope with a point to point resolution of 0.17 nm.

The layer and interfacial structure of the Cu/Co multilayers was investigated using grazing incidence x-ray reflectivity (GIXR). Both specular and diffuse x-ray measurements were carried out on a Bede GXR1 laboratory reflectometer[12] and at station 2.3 of the Synchrotron Radiation Source (SRS) at the CLRC Daresbury Laboratory.[13] The SRS produces a brilliant x-ray beam with the wavelength being selected using a water cooled double bounce Si(111) monochromator. Typical count rates of 10^8 counts/s were achieved in the incident beam. A large projected lateral coherence length, typically 100 μm, was produced due to the large distance between the sample and the source.

Polarized neutron reflectivity (PNR) measurements during magnetization were carried out at the CLRC Rutherford Appleton Laboratory's pulsed neutron source, ISIS, using the polarized neutron mode of the time of flight reflectometer CRISP. A detailed description of the CRISP instrumentation and a discussion of the theory may be found elsewhere.[14]

III. RESULTS AND DISCUSSION

Figure 1 shows some of the GMR values and associated magnetic hysteresis loops of a series of type-B multilayers grown on ion beam etched silicon substrates. The drop in the magnitude of the GMR with increasing etching voltages is striking. The most obvious explanation is that errors in the deposition process are causing a variation in the nonmagnetic spacer thickness. This would tend to shift the multilayer system off the antiferromagnetic peak in the oscillatory coupling curve thus reducing the magnitude of the resistance change. In order that this possibility might be tested a large number of samples were prepared in several series and their magnetoresistance measured. In Fig. 1 we show GMR values for three samples at each etching voltage. In all cases the magnitude of the GMR was found to fall on or beneath an envelope of maximum change indicating that

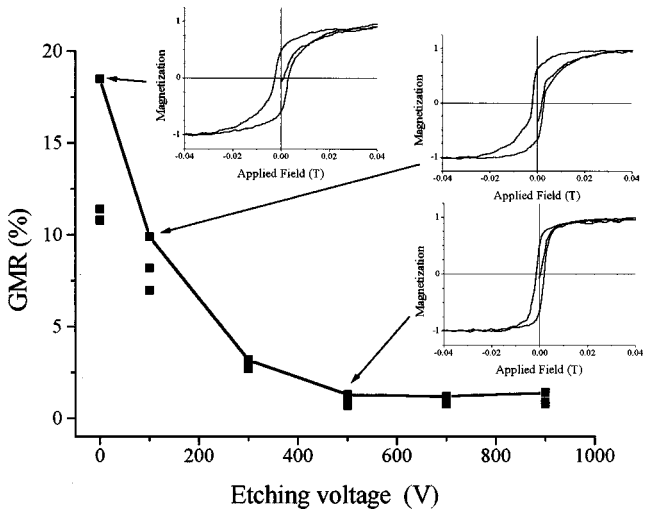

FIG. 1. Variation in GMR and magnetic hysteresis behavior caused by substrate etching in $16\times(1$ nm Co/2 nm Cu)$+1$ nm Pt sputter-deposited multilayers.

the trend has its origins in a source other than spacer thickness variation. Although significant variations from the nominal value of the copper spacer thickness at the second maximum are unlikely, these measurements would allow for and accommodate such a condition. It should also be noted that similar trends in the loss of GMR with substrate etching were observed in this work for type-A multilayers grown on (100) silicon, and also for types A and B grown on (111) silicon. These latter findings also corroborate the results of Pollard *et al.*[11] The hysteresis loop from the multilayer prepared on the unetched substrate, and giving a creditable GMR of about 20% for $t_{Cu}=2$ nm in Fig. 1, shows that the multilayer is clearly not completely antiferromagnetically coupled. However, careful examination of the other hysteresis loops in Fig. 1, shows that, as the ion beam etching energy is increased, the loops become more upright and ferromagnetic in form and lose the contribution from the regions of antiferromagnetic coupling in the multilayer. The remanence changes little as the antiferromagnetic component is lost, the change being masked by the regions of ferromagnetic coupling. The coercivity and, importantly, the saturation field both clearly decrease with increasing etching energy reflecting the easier switching of the magnetization as the antiferromagnetic component reduces. As shown below, PNR confirms this change in magnetic coupling. The GMR seems to saturate, on average, at a minimum value of about 2%. Having established the apparent correlation between GMR and etching voltage in our samples it is necessary to question the origin of the effect. This report is mainly concerned with a detailed structural investigation of these samples since the two most obvious mechanisms for the loss in GMR are (i) changes to any interfacial scattering contribution depending on interface roughness, and (ii) changes to any volume contribution depending on the crystal orientation of the layered structure.

Since the refractive index for materials at x-ray and neutron wavelengths is less than unity, total external reflection occurs at low incidence angles. At incidence wave vectors above some critical value the radiation penetrates deeper into the sample as the angle is increased. Measurement of the

critical angle and of the falloff rate in the intensity yields information on the surface density and roughness. If one or more layers are present in the film near the surface, interference oscillations may be observed in the reflectivity profile. The reflectivity profile is a function of the refractive index, roughness, and thickness of each of the layers in the film and obeys Fresnel's laws.

Neutron reflectivity measurements have two major advantages over x rays. First, neutron scattering amplitudes are not a monotonic function of the atomic number, they vary erratically from element to element. The other is the fact that there is a magnetic contribution to the refractive index in addition to the nuclear one. For materials magnetized in the plane of the sample, neutrons polarized parallel $(+)$ or antiparallel $(-)$ to the applied field have a spin-dependent refractive index. Thus neutron reflectivity is a sensitive probe of the variation in magnetization with depth. Since one would expect to see evidence of antiferromagnetic coupling between the magnetic layers in these films, and the magnetic profile will change on applying a saturation field, the reflectivity curve should exhibit a definite dependence on applied field. Therefore, reflectivity data were taken for each film at 3 mT (guide field only) and at 300 mT (saturation).

Figure 2(a) shows PNR data for an unetched type-B sample taken in a 3 mT guide field. Type-B samples were chosen for the PNR experiments because of their low saturation fields ($\sim$200 mT) as compared to those of type-A samples ($\sim$1 T). Although it is an extremely bright spallation neutron source, the beam intensity at ISIS is orders of magnitude less than that from x-ray sources. Intensity is a particular problem with the CRISP instrument where much of the intensity is lost in the beam refinement and polarization process. For this reason, the sample must have as great a surface area as possible, thus improving the counting statistics. As a consequence of the large sample size, the gap between the pole pieces of the magnet is greater than 80 mm restricting the maximum field obtainable with a conventional water cooled magnet to about 300 mT.

There are a number of features in the PNR curves which attest to the birefringent nature of these magnetic multilayers. The most obvious is the change in the critical reflection scattering vector Q_c seen most clearly in the inset of Fig. 2(a), where, since Q_c is a function of the refractive index and the refractive index is related to the relative orientations of the sample and neutron magnetizations, irradiating the sample alternately with oppositely polarized neutrons will result in a birefringent splitting at the critical edge. Also, at the multilayer Bragg peak q_{Bragg} where the reflectivity is due to constructive interference of reflections from the bilayers, the intensity is related to the scattering potential between the bilayers. Since, because of the magnetic birefringence, the refractive index of cobalt for spin-up neutrons approaches that of copper, the scattering potential will drop causing a reduction in the Bragg peak intensity for spin-up neutrons.

A number of changes become apparent on the application of a saturation field. First, there is a greater difference between $Q_c^{\uparrow}$ and $Q_c^{\downarrow}$ in Fig. 2(a) and, secondly, there is a greater difference in the intensities at the Bragg peak, both of which may be understood in terms of an increase in the magnetization. However, the most relevant change is that seen at q_{mag} which is a half order peak corresponding to a structure with

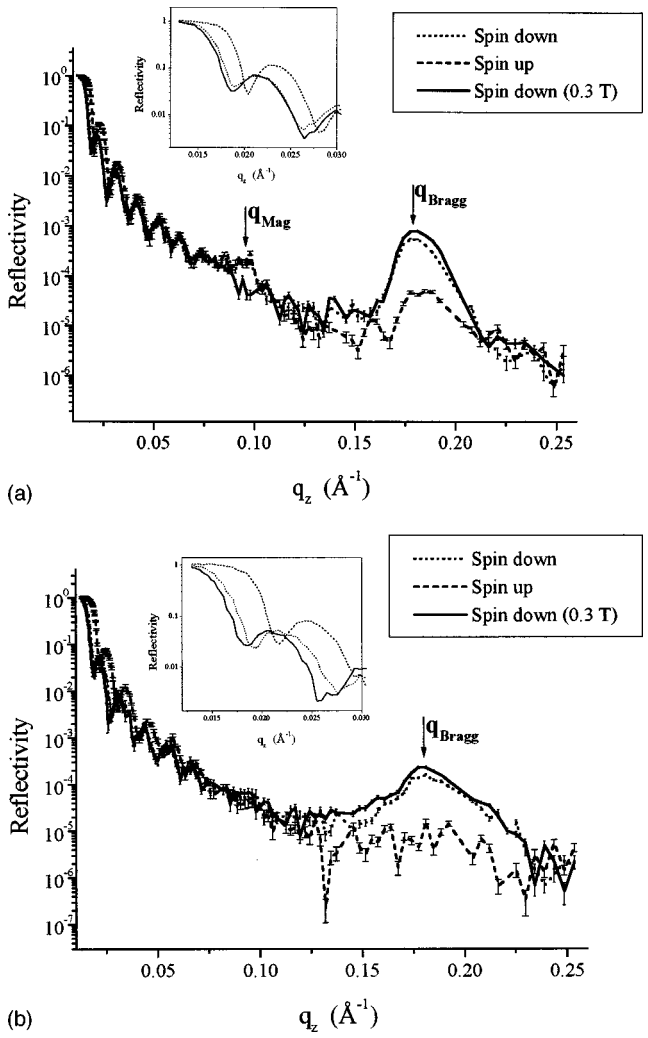

FIG. 2. Specular PNR data for (a) an unetched and (b) an etched type-B sample. The inset shows the divergence of the curves at the critical edge.

a period of double that of the chemical structure. This is indicative of significant antiferromagnetic coupling between the magnetic layers. The magnetic nature of this peak is confirmed when, on changing the magnetic structure from antiferromagnetic to ferromagnetic on application of the 300 mT field, the peak at q_{mag} disappears and the intensity at q_{Bragg} is increased. Similar examination of the etched sample, Fig. 2(b), shows no such changes in the reflectivity profile with applied field except for the slight increase in the Bragg peak which may be attributed to the improvement in magnetic order between the remanent and saturated states. There are some differences, however, between the profiles of etched and unetched samples, which may be attributed to an increase in interfacial roughness and a slight disordering of the layer structure.

In specular x-ray reflectivity scans ($\delta\phi = 2\,\delta\theta$), where the detector is scanned at twice the rate of the sample, $Q(=k_s - k_i)$ is directed normal to the surface and has a magnitude $q_z = (4\pi/\lambda)\sin\theta$. The scattering vector Q is the vector sum of the orthogonal vector components q_x, q_y, and q_z, and in the specular condition $q_x = q_y = 0$. The true specular reflectivity, with a δ function cross section in the q directions normal to the specular ridge is distinct from the diffuse sig-

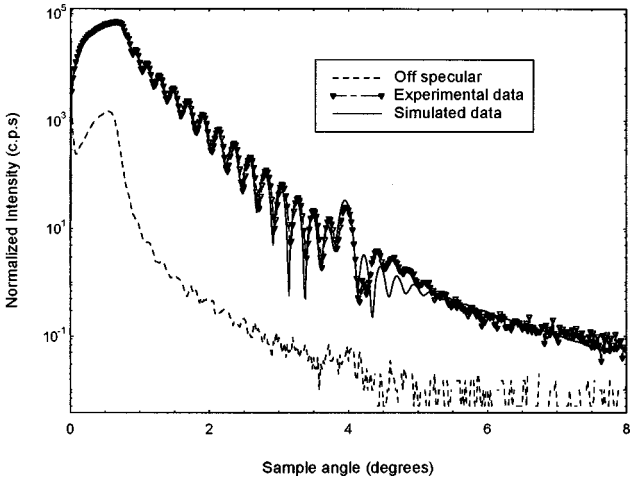

FIG. 3. Specular and off-specular x-ray scan for a 100 V etch type-A sample ($t_{Cu} \sim 1$ nm) showing the presence of correlated roughness, indicated by off specular fringes. The dashed line is the simulated fit to the specular curve.

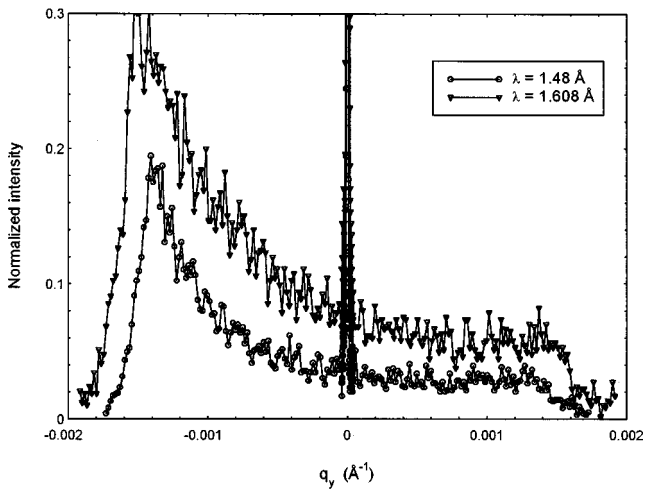

FIG. 4. Transverse diffuse x-ray scans, from the sample of Fig. 3, taken through the first Bragg peak close to and away from the cobalt absorption edge.

nal which has an intrinsic width in reciprocal space but also peaks at the specular ridge. Off-specular longitudinal diffuse scans ($\delta\phi = 2\delta\theta + \Delta$) were used to record the intensity of the diffuse scatter just below the specular ridge. The scan takes the same form as the normal specular scan but with a slight offset, typically 0.1°, in the sample angle. Transverse (q_y) scans in reciprocal space were recorded in which the detector angle was fixed and the specimen scanned.

The tunability of x-ray synchrotron radiation allows scattering from interfaces between elements close in the Periodic Table to be enhanced using anomalous dispersion. The anomalous dispersion correction to the scattering factor changes rapidly with wavelength so it was therefore essential to locate accurately the wavelength with respect to the Cu and Co absorption edges and for this to be reproducible. This was achieved by measuring the fluorescence yield for standard samples as a function of the incident wavelength. Scans were recorded at the Co absorption edge (1.608 Å) and away from it (1.48 Å). Tuning the wavelength to the Co edge considerably enhances the intensity of the first order Bragg peak for systems in which the interfacial roughness is correlated in nature.

Roughness with spatial frequencies copied from lower layers is said to be conformal or correlated. Conformal roughness which is only replicated over a few of the layers will result in an increase of the diffuse scatter around the specular Bragg peak. However, if this roughness is replicated through the whole sample, the diffuse scatter will show periodicity in q_z equal to that of the Kiessig fringes. The extension of the periodicity into q_y, depends on the frequency of the roughness that is being replicated.[15] As low-frequency roughness is the most easily replicated, off-set $\theta/2\theta$ scans with a small q_y component will detect the presence of any correlated roughness. Specular and off-specular scans for a type-A sample etched at 100 V are shown in Fig. 3 and show notable fringes at low angle in the off-specular scan. This, as mentioned above, can be explained by the presence of a high degree of conformal roughness in the multilayer propagating from the substrate upwards. Without the presence of a high degree of conformal roughness these off specular fringes would not be present. Detailed simulations were carried out on the specular and transverse diffuse scans using the Bede Scientific GIXS code.[16] The simulations are based on calculating the scattering from model fractal surfaces using the distorted-wave Born approximation.[16–18] Simulation of specular scans allows layer thickness, near-surface density and an effective roughness to be quantified. Transverse diffuse simulations allow this effective roughness to be distinguished from the true roughness, which itself can be subdivided into correlated and uncorrelated components. Additionally the lateral coherence length ξ and fractal parameter h which characterize the in-plane structure of the interfaces, can be determined.[19]

Figure 4 shows the anomalous scattering data recorded at and away from the cobalt absorption edge (1.608 Å) taken through the first order Bragg peak. There is a change by a factor of 1.5 in the diffuse scatter intensity with wavelength. Transverse scans taken away from the Bragg peak show virtually no increase in intensity. The observation that the Bragg peak diffuse scan intensity increases by tuning the x-ray wavelength to the Co absorption edge is another indication of the highly conformal nature of the interfacial roughness. Diffuse scans taken at the Bragg angle are predominantly sensitive to conformal roughness rather than nonconformal roughness. The enhancement of the diffuse intensity at the Bragg condition, using anomalous dispersion, but not at any other angle infers that the majority of the interfacial roughness is conformal throughout the Cu/Co superlattice.

Specular simulations similar to that shown in Fig. 3 were carried out for a number of type-A samples in order to establish the interfacial characteristics across the series. Figures 5(a) and 5(b) show examples of transverse diffuse scans (rocking curves) and simulated fits. In all cases the simulated data was in good agreement to the recorded data. The simulations show that both the interfacial roughness and bilayer thickness remain relatively constant, within the limit of the errors, across the series independent of the etching voltage. The relevant simulation results are given in Table I. The low ratio of uncorrelated to conformal roughness shows the

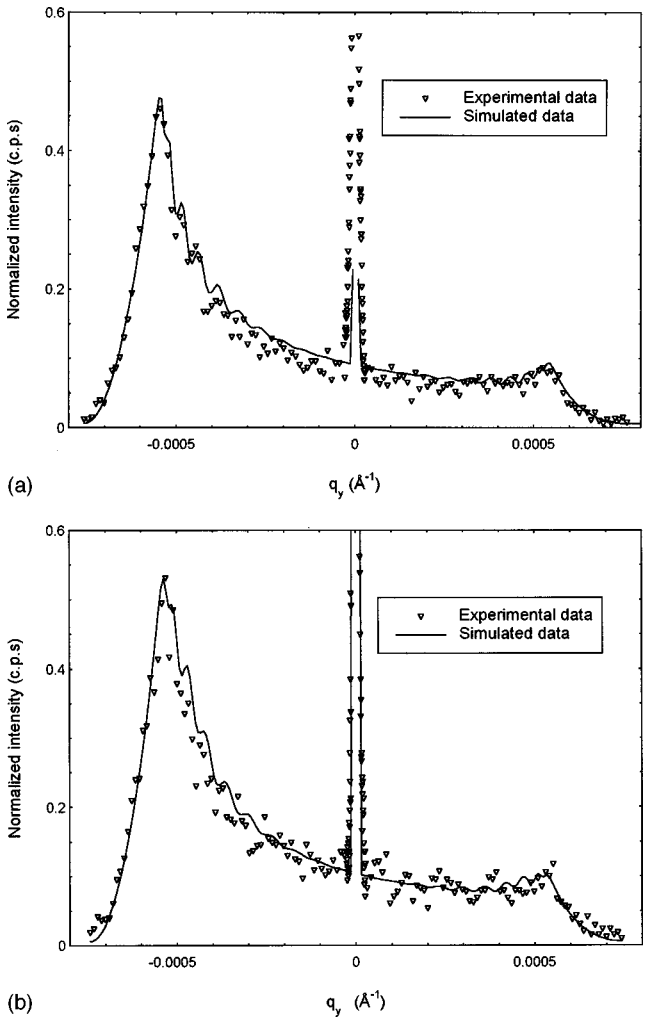

FIG. 5. Transverse diffuse x-ray scans for the 100 V etch type-A sample taken (a) at $\lambda = 1.48$ Å, through a Kiessig minimum $2\theta = 2.713°$ and (b) at $\lambda = 1.608$ Å, through a Kiessig maximum $2\theta = 2.802°$. Scans shows experimental data (triangles) and simulated fit (solid line).

roughness to be predominantly correlated (conformal) throughout the stack and again this does not change across the series. The correlation length is consistently short across the series which means that care must be taken in interpreting any roughness calculations made using the Born wave approximation as it is likely that a substantial fraction of the diffuse scatter will be missed due to the need to probe large q_y in reciprocal space. However, the simulation code used here is based on the distorted-wave Born approximation (DWBA) which takes this into account and therefore, by fitting both diffuse and specular scatter measured in the transverse scans, provides the reliable roughness values shown in Table I.

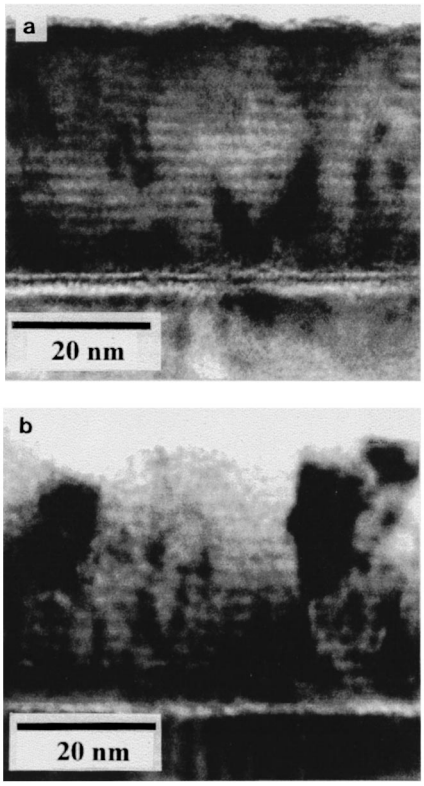

FIG. 6. Defocused TEM cross-sectional micrographs of (a) an unetched type-A sample and (b) a heavily etched type-A sample.

TEM cross-section micrographs provide a more intuitive, if localized, view of the interfacial structures. Figures 6(a) and 6(b) show a pair of defocused micrographs of an unetched and a heavily etched type-A sample ($t_{Cu} \sim 1$ nm), respectively. The microscope is defocused to enhance the phase contrast between the Co and Cu layers, thus revealing the layered structure. The Si substrate is below the multilayer and at the bottom of the two micrographs. The natural SiO_2 layer between the unetched Si and the superimposed multilayer is clearly visible in Fig. 6(a). The substrate has been etched in Fig. 6(b) but there still appears to be some form of amorphous layer between the Si and the Co/Cu structure. The similarity between the multilayer images in the two micrographs is striking and in agreement with the x-ray modeling results, although direct comparisons are difficult because of the increased strain contrast in the heavily ''etched'' film. They, and Fig. 7 below, show the lateral

TABLE I. X-ray modeling parameters for sputtered Cu/Co multilayers.

Etching energy (V)	Cu spacer thickness (nm)	Roughness, σ (nm)	Correlation length $\check{\zeta}$ (nm)	Fractal parameter h	uncorrelated/conformal roughness
0	1.05±0.05	0.54±0.05	8.5±0.5	0.9±0.1	0.29±0.02
100	1.07±0.05	0.52±0.05	8.5±0.5	0.9±0.1	0.29±0.02
300	1.02±0.05	0.54±0.05	10.0±0.5	0.9±0.1	0.29±0.02
500	1.05±0.05	0.51±0.05	11.8±0.5	1.0±0.1	0.29±0.02

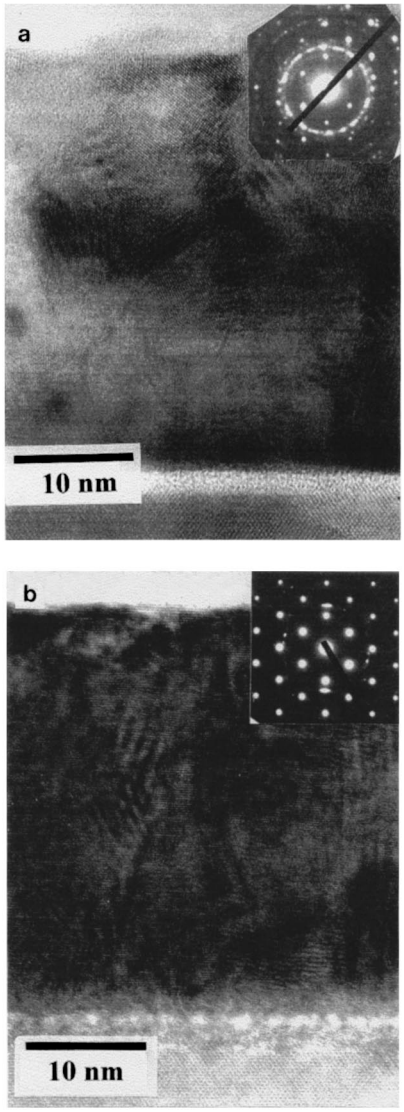

FIG. 7. Cross-sectional TEM micrograph of (a) an unetched and (b) an etched type-A film with the inset showing the TED pattern containing reflections (spots) from the Si substrate and diffraction features from the multilayer.

correlation length of the surface roughness and quantitative measurements confirm it to be of the order of that found in the x-ray simulations. The images also show that the interfaces between the Co and Cu layers are quite sharp suggesting that it is the long length scale rippling of the layers which contributes to the rms roughness values. This illustrates the importance of conformality in the multilayer stack. As long as the roughness is conformal through the stack, the separation between magnetic and nonmagnetic spacers is preserved thus maintaining one of the principal prerequisites for GMR.

Focused TEM cross-sectional micrographs and TED patterns for the type-A films are shown in Fig. 7. Since the scattering factors for Co and Cu are similar, it is not possible to see any layer contrast in either of the images. However, the changes in bulk texture with substrate etching are very clear. Figure 7(a) shows an unetched type-A sample where the diffraction pattern contains the silicon spots (on the [110] zone axis) from the substrate and the first diffraction orders from a random polycrystalline fcc microstructure in the

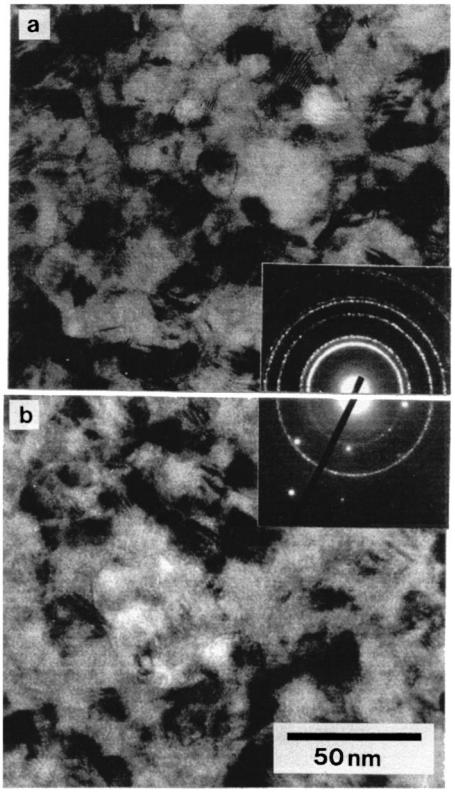

FIG. 8. In-plane TEM micrograph and associated TED pattern from (a) an unetched and (b) an etched type-B multilayer.

multilayer. The rings are not completely continuous because, with the small diffraction aperture used, there is a restricted number of grains being sampled by the electron beam. The Si substrate with its native oxide is visible in the micrograph as are the resolved Si{111} lattice fringes. The etched sample, Fig. 7(b), is very different. Here the diffraction by the film is limited to short {111} arcs along the [001] Si direction (i.e., diffraction from {111} Co/Cu planes parallel to the film plane of the multilayer). Examination of the lattice fringe contrast from the multilayer in the micrograph shows that, although the texture does not correspond exclusively to {111} grains oriented parallel to the substrate and the interfaces of the multilayer, a significant fraction of the film is growing with a strong ⟨111⟩ fiber axis. In-plane micrographs with most of the substrate removed, Figs. 8(a) and 8(b), show the grain size in the multilayer to be about 20–30 nm, and roughly the same in both the unetched and etched samples. They also show the transition from a random polycrystalline structure in Fig. 8(a) to a mosaic structure with a preferred growth along the ⟨111⟩ direction in Fig. 8(b). The intensities of the rings in the inset diffraction pattern in Fig. 8(a) are typical of a randomly oriented fcc microstructure while the strong {220} ring, and the much reduced intensities or absence of the other reflections in Fig. 8(b), is consistent with a very strong ⟨111⟩ fiber texture.

This change in texture is confirmed by HXRD in Fig. 9 which shows patterns from unetched and etched B-type samples. For the etched sample there is a clear increase in the intensity of the compromise {111} Co/Cu peak over that for the unetched sample by a factor of between 20 and 30. There is also a concurrent disappearance of the small {200} peak at $2\theta \approx 51°$. The presence of the multilayer satellite maxima

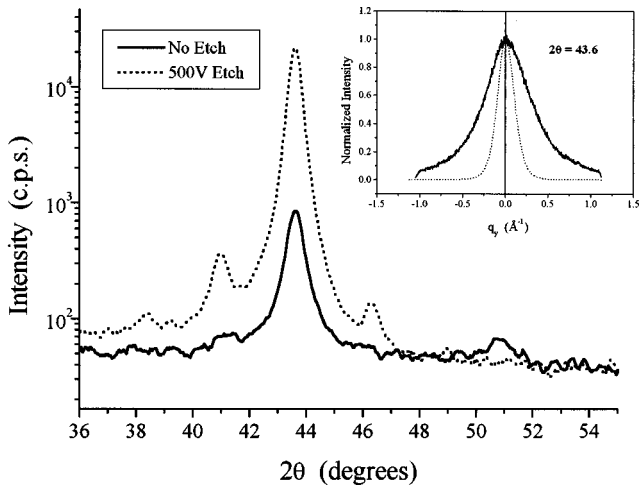

FIG. 9. HXRD data from an etched and an unetched type-B multilayer. The inset shows rocking curves taken about the compromise {111} Co/Cu peak.

clearly visible around the stronger {111} reflection are a further indication that the layer integrity is strongly maintained in the etched sample. The inset shows rocking curves taken at the {111} Co/Cu peak for the same two samples with the full width at half maximum decreasing with increasing etching energy. The sharp reduction in half width, corresponding to a reduced mosaic spread out of the film plane with increase in etching voltage, further supports the argument that the etching process encourages the formation of a strongly textured ⟨111⟩ fiber axis microstructure in the multilayers.

IV. CONCLUSION

We have shown that ion beam etching of the substrate has a major effect on the magnitude of the GMR in Co/Cu multilayers sputter-deposited on silicon substrates [in this paper (100)Si and in Ref. 11 (111)Si]. In our previous work, and in this report, we have shown that this change is associated with a transformation of the crystalline texture of the Co/Cu multilayer thin films. HXRD and high-resolution TEM and TED investigations have shown conclusively that as the etching energy is increased the texture is transformed from a randomly oriented polycrystalline film into a well oriented ⟨111⟩ polycrystalline film. This is accompanied by a decrease in the volume fraction of grains otherwise oriented, particularly in ⟨100⟩. The presence of this relatively small fraction of ⟨100⟩ oriented grains may be crucial for the appearance of a significant GMR. Their presence can be easily missed unless careful diffraction experiments are performed.[20] In the change to the oriented microstructure, magnetic, and PNR measurements show a concomitant loss of the fraction of antiferromagnetic coupling in the multilayers as the etching voltage increases. GIXR investigations, matched with careful and detailed modeling calculations, show no significant change in interfacial roughness with etching. In agreement with the TEM observations, they show that this roughness is conformal and is largely correlated throughout the thickness of the multilayer.

It would seem therefore that the likely loss of GMR in our samples is related to crystallographic orientation changes and bulk scattering, i.e., spin-dependent *s*-*d* scattering into the split *d* band in the ferromagnetic layers, rather than changes in interfacial roughness and interfacial scattering. A similar conclusion as to the relative importance of *s*-*d* scattering in the Co/Cu system has recently been published.[21] Many previous investigations, e.g., Ref. 22, have shown that enhanced GMR is obtained in Co/Cu multilayers sputter-deposited on Fe underlayers. This promotes a ⟨200/220⟩ texture and a large GMR, whereas fcc underlayers encourage ⟨111⟩ growth and a low GMR. The substrate etching experiments reported here clearly provide the required interfacial energy match for the growth of a very strong ⟨111⟩ texture.

It is obvious that we cannot comment, from the results presented in this report, on any effect that changed interfacial roughness would have on GMR, since the interfacial roughness of our samples is relatively constant across the series. However, as mentioned in the Introduction, GMR measurements on Co/Cu multilayers with interfaces roughened by sputtering at different argon pressures[8] do show a correlation with this roughness, estimated from broadening of the first Bragg multilayer diffraction maximum. Minimum roughness $\sigma_{\mathrm{rms}}\sim 1.6$ nm corresponded to maximum GMR. There is also an inferred dependence on texture with a ⟨200/220⟩ texture giving the best GMR. Recent measurements[23] on sputter-deposited and relatively randomly oriented Co/Cu multilayers with extremely flat interfaces at $\sigma_{\mathrm{rms}}\sim 0.1$ nm, show dramatically large GMR.

ACKNOWLEDGMENTS

The authors would like to thank J. Penfold, D. Bucknall, and S. Langridge for assistance with the PNR measurements and RAL for time on the CRISP instrument. We also wish to thank Mr. Brian Ashworth for his assistance with the TEM sample preparation. EPSRC is acknowledged for Grant No. GR/H65320 providing the JEOL 3010 TEM.

[1] M. N. Baibich, J. M. Broto, A. Fert, F. Nguyen Van Dau, F. Petroff, P. Etienne, G. Creuzet, A. Friederich, and J. Chazelas, Phys. Rev. Lett. **61**, 2472 (1988).

[2] D. M. Edwards, J. Mathon, and R. B. Muniz, IEEE Trans. Magn. **27**, 3548 (1991).

[3] S. S. P. Parkin, R. Bhadra, and K. P. Roche, Phys. Rev. Lett. **66**, 2152 (1991).

[4] P. Bruno and C. Chappert, Phys. Rev. Lett. **67**, 1602 (1991).

[5] W. F. Egelhoff and M. T. Kief, IEEE Trans. Magn. **28**, 2742 (1992).

[6] D. Greig, M. J. Hall, C. Hammond, B. J. Hickey, H. P. Ho, M. A. Howson, M. J. Walker, N. Wiser, and D. G. Wright, J. Magn. Magn. Mater. **110**, L239 (1992).

[7] J. J. de Miguel, A. Cebollada, J. M. Gallego, R. Miranda, C. M. Schneider, P. Schuster, and J. Kirschner, J. Magn. Magn. Mater. **93**, 1 (1991).

[8] J. Ben Youssef, K. Bouziane, O. Koshkina, H. Le Gall, M. El Harfaoui, M. El Yamani, J. M. Desvignes, and A. Fert, J. Magn. Magn. Mater. **165**, 288 (1997).

[9] S. K. J. Lenczowski, M. A. M. Gijs, J. B. Giesbers, R. J. M. van

de Veerdonk, and W. J. M. de Jonge, Phys. Rev. B **50**, 9982 (1994).

[10] M. J. Hall, B. J. Hickey, M. A. Howson, M. J. Walker, J. Xu, D. Greig, and N. Wiser, Phys. Rev. B **47**, 12 785 (1993).

[11] R. J. Pollard, M. J. Wilson, and P. J. Grundy, J. Magn. Magn. Mater. **151**, 139 (1995).

[12] N. Loxley, A. Monteiro, M. L. Cooke, D. K. Bowen, and B. K. Tanner, in *Advanced III V Compound Semiconductor Growth, Processing and Devices*, edited by S. J. Pearton, D. K. Sudana, and J. M. Zavada, MRS Symposia Proceedings No. 240 (Materials Research Society, Pittsburgh, 1992), p. 219.

[13] URL http://wserv1.dl.ac.uk/SRS/XRD/2.3.dir/; R. J. Cernik, P. K. Murray, P. Pattison, and A. N. Fitch, J. Appl. Crystallogr. **23**, 292 (1990); S. P. Collins, R. J. Cernik, P. Pattison, A. M. T. Bell, and A. N. Fitch, Rev. Sci. Instrum. **63**, 1013 (1992).

[14] J. Penfold, Physica B **173**, 1 (1991); C. F. Majkrzak, *ibid.* **173**, 75 (1991); URL:http//ndafleetwood.nd.rl.ac.uk/largescale/crisp/CRISP.htm.

[15] V. Holý, J. Kuběna, I. Ohlídal, K. Lischka, and W. Plotz, Phys. Rev. B **47**, 15 896 (1993).

[16] B. K. Tanner, M. Wormington, T. P. A. Hase, and I. Pape, *Physics, Chemistry and Mechanics of Surfaces* (Gordon and Breach, New York, 1996).

[17] M. K. Wormington, K. Sakurai, D. K. Bowen, and B. K. Tanner, in *Determining Nanoscale Physical Properties of Materials by Microscopy and Spectroscopy*, edited by M. Sarikaya, M. Isaacson, and H. K. Wickramasighe, MRS Symposia Proceedings No. 332 (Materials Research Society, Pittsburgh, 1994), p. 525.

[18] M. Wormington, I. Pape, T. P. A. Hase, B. K. Tanner, and D. K. Bowen, Philos. Mag. Lett. **74**, 211 (1996).

[19] S. K. Sinha, E. B. Sirota, S. Garoff, and H. B. Stanley, Phys. Rev. B **38**, 2297 (1988).

[20] J. Langer, R. Mattheis, S. Schmidt, St. Senz, and T. Zimmermann, J. Magn. Magn. Mater. **156**, 19 (1996).

[21] M. J. Hall, D. B. Jardine, J. E. Evetts, J. A. Leake, and R. E. Somekh, J. Magn. Magn. Mater. **173**, 253 (1997).

[22] P. J. Grundy, R. J. Pollard, and M. E. Tomlinson, J. Magn. Magn. Mater. **126**, 516 (1993).

[23] C. H. Marrows, N. Wiser, B. J. Hickey, T. P. A. Hase, B. K. Tanner, and C. W. Lehmann (private communication); (unpublished).